


Article

Mo-Doped Cu₂S Multilayer Nanosheets Grown In Situ on Copper Foam for Efficient Hydrogen Evolution Reaction

Yajie Xie ^{1,2}, Jianfeng Huang ^{1,2,*}, Rui Xu ², Danyang He ², Mengfan Niu ², Xiaoyi Li ², Guoting Xu ², Liyun Cao ² and Liangliang Feng ^{1,2,*} 

¹ Key Laboratory of Auxiliary Chemistry and Technology for Chemical Industry, Ministry of Education, Shaanxi University of Science and Technology, Xi'an 710021, China

² School of Material Science and Engineering, International S&T Cooperation Foundation of Shaanxi Province, Shaanxi University of Science and Technology, Xi'an 710021, China

* Correspondence: huangjf@sust.edu.cn (J.H.); fengll@sust.edu.cn (L.F.)

Abstract: Metal sulfide electrocatalyst is developed as a cost-effective and promising candidate for hydrogen evolution reaction (HER). In this work, we report a novel Mo-doped Cu₂S self-supported electrocatalyst grown in situ on three-dimensional copper foam via a facile sulfurization treatment method. Interestingly, Mo-Cu₂S nanosheet structure increases the electrochemically active area, and the large fleecy multilayer flower structure assembled by small nanosheet facilitates the flow of electrolyte in and out. More broadly, the introduction of Mo can adjust the electronic structure, significantly increase the volmer step rate, and accelerate the reaction kinetics. As compared to the pure Cu₂S self-supported electrocatalyst, the Mo-Cu₂S/CF show much better alkaline HER performance with lower overpotential (18 mV at 10 mA cm⁻², 322 mV at 100 mA cm⁻²) and long-term durability. Our work constructs a novel copper based in-situ metal sulfide electrocatalysts and provides a new idea to adjust the morphology and electronic structure by doping for promoting HER performance.



Citation: Xie, Y.; Huang, J.; Xu, R.; He, D.; Niu, M.; Li, X.; Xu, G.; Cao, L.; Feng, L. Mo-Doped Cu₂S Multilayer Nanosheets Grown In Situ on Copper Foam for Efficient Hydrogen Evolution Reaction. *Molecules* **2022**, *27*, 5961. <https://doi.org/10.3390/molecules27185961>

Academic Editors: Jin Jia and Yucheng Lan

Received: 24 August 2022

Accepted: 10 September 2022

Published: 13 September 2022

Publisher's Note: MDPI stays neutral with regard to jurisdictional claims in published maps and institutional affiliations.



Copyright: © 2022 by the authors. Licensee MDPI, Basel, Switzerland. This article is an open access article distributed under the terms and conditions of the Creative Commons Attribution (CC BY) license (<https://creativecommons.org/licenses/by/4.0/>).

Keywords: Mo doping; Cu₂S; electrocatalyst; hydrogen evolution

1. Introduction

Nowadays, in order to alleviate the non-renewable fossil energy and the associated serious environmental pollution, clean and sustainable energy has been vigorously pursued all over the world. Hydrogen gas, as a green, renewable, high calorific value of combustions and pollution-free energy carrier was widely concerned [1–4]. Among the current three main methods of hydrogen production, water electrolysis is considered to be an ideal pathway with zero-emission, high purity, and abundant water reserves. It is well known that noble metal platinum (Pt) and platinum-based materials offer the most efficient and stable electrocatalytic activity [5,6]. However, the scarcity and high cost of platinum (Pt) seriously limit its practical deployment. Thus, it is urgent to develop new high-performance and cost-effective electrocatalysts for hydrogen evolution reaction (HER).

Benefitting from the d-orbital electrons and vacant d-orbitals simultaneously existing in transition metal, it is easy to lose or capture electrons and has strong capable of redox reaction, which can bring down the activation energy of the water-splitting-related intermediates generated and thus promote the electrocatalytic process. Until now, transition metal-based electrocatalysts, including phosphides [7–11], (hydro) oxides [12,13], selenides [14,15], etc., have attracted much attention. Among them, transition metal sulfides (TMS) have been exploited by untiring effort as a considerably promising electrocatalyst in view of their advantages of economy and excellent electrochemical performance on water splitting [16–19]. Compared with Fe, Co and Ni, Cu was recognized as having favorable stability, excellent electrical conductivity and cost effectiveness; therefore, copper sulfide has been widely investigated in energy storage and conversion fields, such

as battery [20,21], capacitor [22,23] and photocatalysis [24,25]. For example, Zhu et al. synthesized hierarchical cuprous sulfide nanosheets to modify nanowires on copper foam as a non-binder conversion cathode material for lithium/magnesium hybrid battery [20]. Li et al. successfully exploited multistage hybrid cuprous sulfide (Cu_2S) nanoparticles anchoring on graphene to improve capacitive energy storage [22]. Wang et al. constructed cuprous sulfide nanoparticles for photocatalytic reduction of carbon dioxide on amorphous CuS_x matrix and successfully boosted the catalysis of cuprous sulfide with hybrid structure [24]. However, cuprous sulfide (Cu_2S) is rarely used in the realm of electrochemical hydrogen evolution [26–28]. Zhang et al. proposed a “d-orbital complementarity” principle for the synthesis of vanadium-doped cobalt phosphide (V-CoP) as an efficient electrocatalyst towards HER [29]. Inspired by the “d-orbital complementarity” principle, we aim to develop a simple and universal method such as doping the early transition metal Mo to cuprous sulfide, which possesses the late transition metal copper. We aim to modulate the electronic structure and nano-structure, increase the specific surface area of catalysts, and enhance catalytic activity. Thus, the high-cost challenge may be alleviated, making it promising in use in large-scale and highly efficient water electrolysis.

In this report, molybdenum doped Cu_2S multilayer nanosheets grown in situ on copper foam (CF) were synthesized by one-step hydrothermal route, denoted as Mo- $\text{Cu}_2\text{S}/\text{CF}$. The results show that the molybdenum doping changed the nano-structure of the catalyst and formed a fluffy multilayer flower-like structure, leading to enlarging more active surface area, and promoted the optimization of electronic structure for improved intrinsic activity. The optimized Mo- $\text{Cu}_2\text{S}/\text{CF}$ exhibited extraordinarily low HER overpotential and robust stability in alkaline solution which only required 18 mV and 322 mV overpotential for obtaining a high current density of 10 and 100 mA cm^{-2} , and worked stably for at least 20 h. Our work shows an innovative way to design and fabricate potential metal sulfide electrocatalytic materials for hydrogen production in water splitting.

2. Results and Discussion

Molybdenum doped Cu_2S multilayer nanosheets grown in situ on copper foam (Mo- $\text{Cu}_2\text{S}/\text{CF}$) is fabricated by a facile one-step sulfurization hydrothermal method with sulfur source thioacetamide in a hydrothermal system at 180 °C for 24 h, as illustrated in Figure 1. The surface of CF was coarsened by sulfurization etching, which was more conducive to the growth of self-supported electrode, and the Cu^{2+} ions from CF are precipitated into the solution reacting with S^{2-} ions, meanwhile with the successful doping of molybdenum source, Mo- Cu_2S nanosheet array was successfully grown on the CF. The SEM images in Figure 2 clearly reveal that hydrothermal reaction time has a significant impact on the structure and morphology of Mo- $\text{Cu}_2\text{S}/\text{CF}$. When the hydrothermal reaction time is 6 h (Figure 2A), the CF surface is completely covered with the agglomerated balls. With the increase of reaction time 12 h (Figure 2B), small numbers of nanosheets can be observed on the surface of the agglomeration. Extending reaction time to 24 h (Figure 2C), the nanosheet with curved edge can be observed clearly. Obviously, the puffy multilayer nanosheet structure expands the contact area, facilitates the electron transfer rate and the electrolyte in and out. As the reaction time is prolonged to 36 h (Figure 2D), the nanosheets gradually disappear, which is not conducive to the electrolysis reaction to some extent. The phase of Mo- $\text{Cu}_2\text{S}/\text{CF}$ -6 h, Mo- $\text{Cu}_2\text{S}/\text{CF}$ -12 h, Mo- $\text{Cu}_2\text{S}/\text{CF}$ -24 h, Mo- $\text{Cu}_2\text{S}/\text{CF}$ -36 h remains Mo- Cu_2S , as demonstrated in Figure S1.

Figure 3A displays the X-ray diffraction (XRD) spectra of Mo- $\text{Cu}_2\text{S}/\text{CF}$ and $\text{Cu}_2\text{S}/\text{CF}$ exhibited three typical diffraction peaks at 38.33°, 45.17°, 47.76° matches well with Cu_2S (PDF#83-1462), and the two obvious peaks at 43.41° and 50.56° belong to the substrate Cu (PDF#65-9743). This reveals that Cu_2S has good crystallinity, and an “all in one” structured $\text{Cu}_2\text{S}/\text{CF}$ is successfully synthesized. The TEM image of Mo- $\text{Cu}_2\text{S}/\text{CF}$ is observed in Figure 3B, Mo- $\text{Cu}_2\text{S}/\text{CF}$ is composed of many stacked nanosheet structures, which is consistent with SEM images. The HRTEM was also conducted in Figure 3C, a clear lattice spacing ~0.24 nm and ~0.274 nm corresponding to (111) and (034) planes of Cu_2S (PDF#72-

1071) and (PDF#83-1462) respectively consists well with the XRD results. Further, the EDS mapping images of Mo-Cu₂S/CF clearly confirms that Cu, Mo, and S elements are uniformly dispersed over the entire area of nanosheet, resulting in the formation of Mo-doped Cu₂S material (Figure 3D).

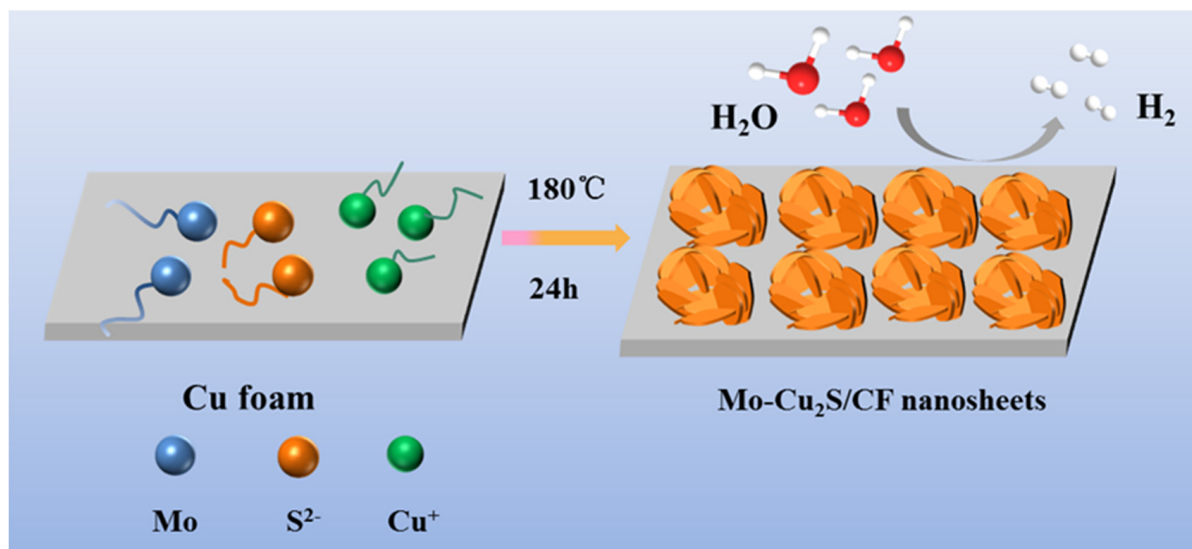


Figure 1. Schematic illustration of the construction of Mo-Cu₂S/CF.

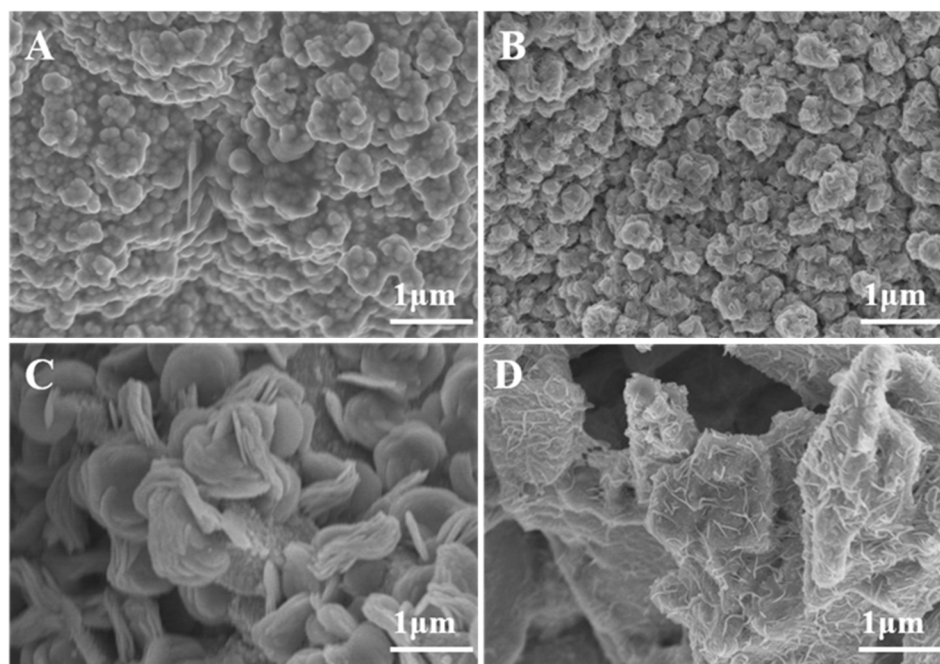


Figure 2. SEM images of Mo-Cu₂S/CF (A) 6 h; (B) 12 h; (C) 24 h; (D) 36 h.

As a comparison, the SEM, TEM and HRTEM images of Cu₂S/CF are performed in Supporting Information. The SEM image of Cu₂S/CF (Figure S2A) displays a block structure with much larger size compared to Mo-Cu₂S/CF, and this is evident in the TEM image (Figure S2B). To further determine the microstructure of Cu₂S/CF, the HRTEM image of Cu₂S/CF is conducted (Figure S2C), and visible lattice fringes with spacing of 0.274 nm are matched with Cu₂S (111) plane. The corresponding elemental mapping images (EDX) of Cu₂S/CF indicate that Cu and S are uniformly distributed over the whole Cu₂S/CF, implying a homogeneous sulfurization (Figure S2D–F). By comparing Figures 3, S2 and S3

and Table S1, it is easy to draw a conclusion that Mo element was successfully induced and played a crucial role in the formation of nanosheet structure, reduced the size of Cu_2S which is conducive to fully exposing active sites on the catalyst surface and making the hydrogen evolution process more efficient. Compared with massive block structures of $\text{Cu}_2\text{S}/\text{CF}$, $\text{Mo-Cu}_2\text{S}/\text{CF}$ with the large fleecy multilayer flower-like morphologies assembled by small nanosheet obviously exposes more active sites and facilitates the flow of electrolyte in and out, effectively improving the efficiency of electrocatalytic hydrogen evolution [30].

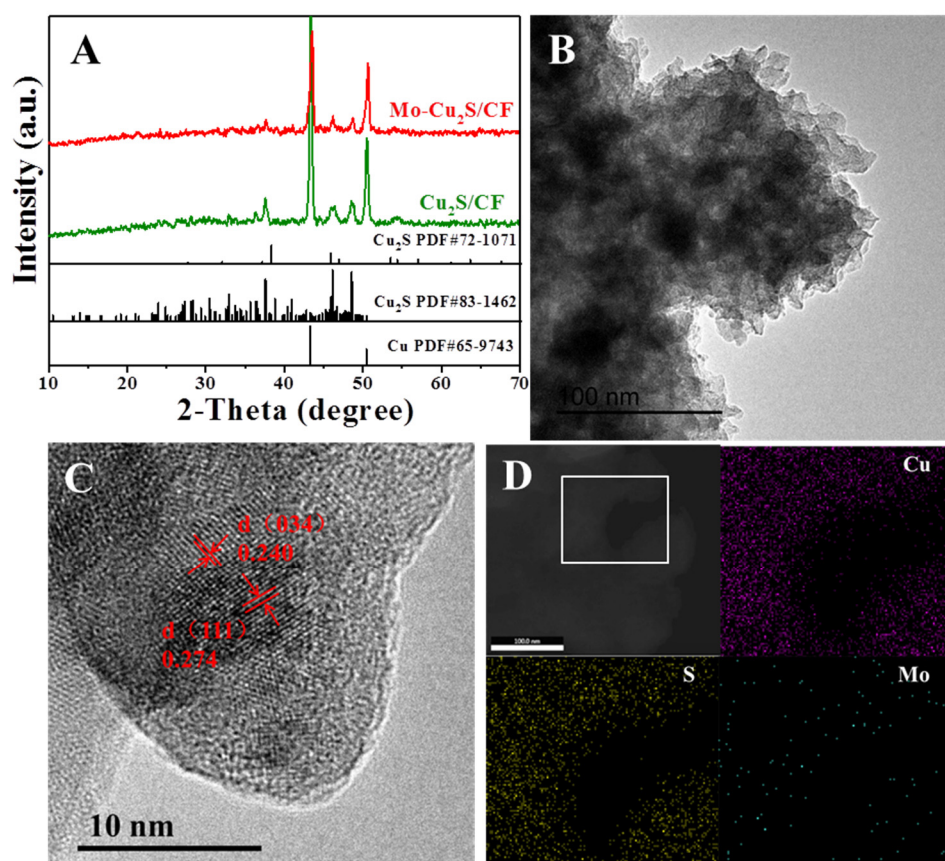


Figure 3. (A) XRD patterns of $\text{Mo-Cu}_2\text{S}/\text{CF}$ and $\text{Cu}_2\text{S}/\text{CF}$; (B) TEM image; (C) the HRTEM image of $\text{Mo-Cu}_2\text{S}/\text{CF}$; (D) the elemental mapping images.

In addition, X-ray photoelectron spectroscopy (XPS) measurements were utilized to elucidate the electronic structure and chemical states on the surface of $\text{Mo-Cu}_2\text{S}/\text{CF}$ and $\text{Cu}_2\text{S}/\text{CF}$ samples. Cu, S, C, O elements of $\text{Mo-Cu}_2\text{S}/\text{CF}$ and $\text{Cu}_2\text{S}/\text{CF}$ are clearly observed in Figure 4A, while the Mo 3d signal appears in $\text{Mo-Cu}_2\text{S}/\text{CF}$, indicating that Mo is successfully doped in the $\text{Cu}_2\text{S}/\text{CF}$ sample. Oxygen signal originates from the surface oxidation in the air. For the case of high-resolution of Cu 2p (Figure 4B), the spectrum clearly displays the Cu $2p_{3/2}$ peaks at 932.43 eV and 934.18 eV [31], which corresponds to Cu^+ and Cu^{2+} states, respectively. The peaks of Cu $2p_{1/2}$ located at 952.28 and 954.34 eV belong to states of Cu^+ and Cu^{2+} . The satellite peaks at 941.32, 944.09 and 962.38 eV confirmed the existence of Cu^{2+} , which is caused by exposure to air [32–34]. To be noticed, Cu $2p_{3/2}$ at 932.43 and 934.18 eV exhibit negative shifts of ~ 0.21 , ~ 0.65 eV, respectively, compared with $\text{Cu}_2\text{S}/\text{CF}$ (952.28 and 954.34 eV), which could lead to the buildup of negative charges on and therefore favoring the adsorption of H^+ intermediates [35–37]. The in-situ Cu^{2+} reduction into Cu^+ ions could be caused by S^{2-} ions reducing agents of $\text{Mo-Cu}_2\text{S}/\text{CF}$ [38]. Meanwhile, we observed that the characteristic peak of Cu^+ $2p_{3/2}$ increases conspicuously in intensity along with the intensity area enlarging from 1.74% to 11.78% compared with $\text{Cu}_2\text{S}/\text{CF}$. These results demonstrate that $\text{Mo-Cu}_2\text{S}/\text{CF}$ has better HER

performance because Cu^+ species have easier electron transfer than Cu^{2+} [27]. Figure 4C shows the comparison of S 2p XPS spectrum among Mo-Cu₂S/CF and Cu₂S/CF. There are two characteristic peaks with energy of 161.7 and 162.94 eV that can be assigned to S 2p_{3/2} and S 2p_{1/2} [39], indicating the formation of metal sulfides. The weak peak at 168.52 eV corresponds to SO_4^{2-} , which roots in the surface oxidation of Cu₂S in the air [40]. The binding energies of S 2p peaks in Mo-Cu₂S/CF have positive shifts of ~0.11, ~0.13 eV, as compared to Cu₂S/CF (161.59 and 162.81 eV). Figure 4D demonstrates the successful synthesis of Mo-Cu₂S/CF because the two characteristic peaks at 230.23 and 232.11 eV belong to Mo^{4+} 3d_{5/2} and Mo^{4+} 3d_{3/2}, respectively. Additionally, the higher energy peak at 235.15 eV is indexed to Mo^{6+} , because of the slight oxidation of the sample when exposed to air. From the binding energy deviation of Cu and S, we can conclude that electrons are transferred from S to Cu, indicating that the doping of Mo changes the electronic structure of Cu₂S/CF successfully, and confirming strong electronic interaction between Mo and Cu₂S, which can lead to enhancing electrical conductivity of the material [28,40]. The doping of molybdenum changes the content of Cu^+ , the increasing Cu^+ is more conducive to hydrogen evolution reaction.

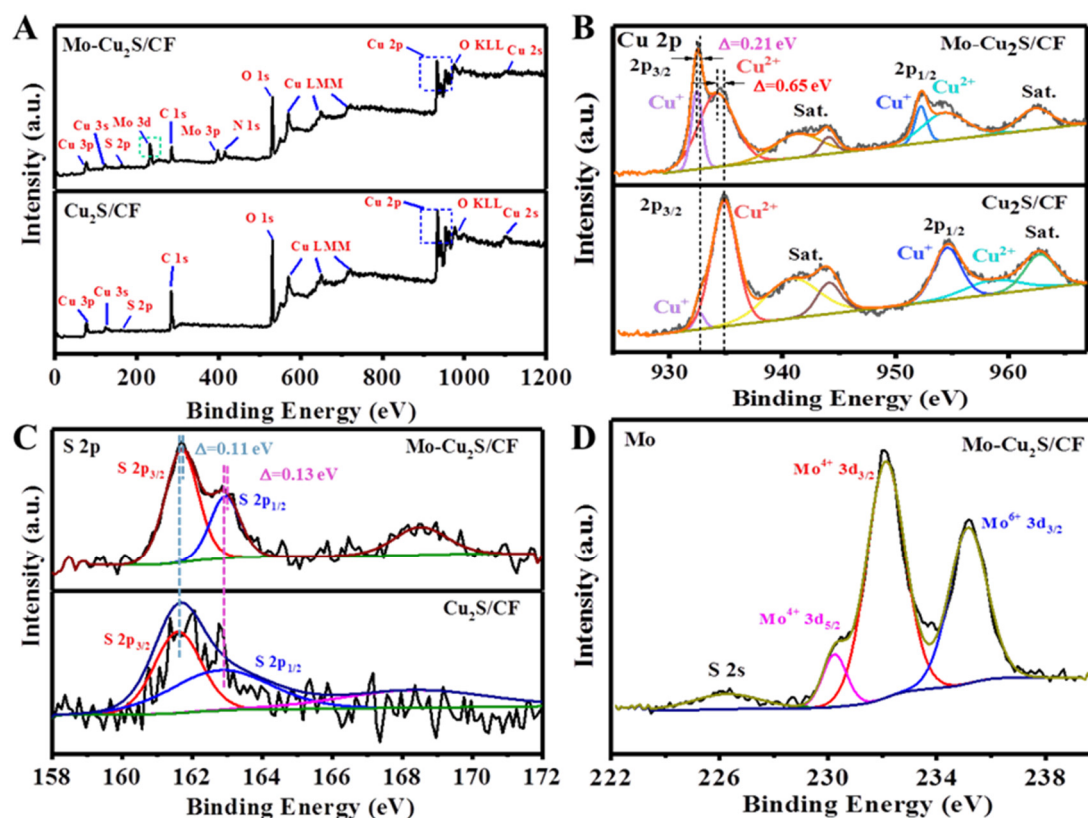


Figure 4. (A) Survey; (B) Cu 2p, (C) S 2p XPS spectra of Mo-Cu₂S/CF and Cu₂S/CF; (D) Mo XPS spectra of Mo-Cu₂S/CF.

The electrocatalytic HER activity of Mo-Cu₂S/CF was tested in Figure 5. Linear sweep voltammetry (LSV) measurements were recorded in 0.1M KOH solution at scan rate of 5 mV s⁻¹. For comparison, the electrochemical hydrogen evolution tests of four samples with different hydrothermal times are carried out respectively (Figure S4). Mo-Cu₂S/CF-24 exhibits best electrocatalytic activity towards HER, with quite a small overpotential of 18 and 322 mV to deliver a current density of 10 and 100 mA cm⁻². In order to verify that the HER activity is driven by the catalytic site on Mo-Cu₂S/CF, the blank CF and Cu₂S/CF are tested respectively. As shown in Figure 5A, Mo-Cu₂S/CF exhibits remarkable HER activity in alkaline media, which requires only a quite small overpotentials of 18/322 mV to deliver the current densities of 10/100 mA cm⁻², and significantly outperforms Cu₂S/CF

(277/445 mV). It was worth noting that the electrocatalytic HER performance over the resultant Mo-Cu₂S was better than that of most of previously reported Cu₂S-based electrocatalyst for HER (Table S2) [26,27,41–47]. Furthermore, the HER kinetics of electrocatalysts are studied in the reference of Tafel slopes in Figure 5B. The Tafel slope of Mo-Cu₂S/CF is 171 mV dec⁻¹, smaller than that of Cu₂S/CF (181 mV dec⁻¹) and pure CF (420 mV dec⁻¹), suggesting that Mo-Cu₂S/CF proceeds the rapidest HER kinetics among them. Electrochemical impedance spectroscopy (EIS) is then examined to reveal electron transfer rates during the HER process. The corresponding Nyquist plots are shown in Figure 5C. Mo-Cu₂S/CF exhibits a smaller charge transfer resistance compared to Cu₂S/CF and pure CF, which indicates that Mo-Cu₂S/CF shows the faster electron transfer and HER kinetics than Cu₂S/CF and pure CF. Electrochemical specific surface area (ECSA) is also an important parameter to estimate the electrochemical properties, which is proportional to double-layer capacitance (C_{dl}). The C_{dl} values of different electrodes are calculated by fitting the plots of current density at different scan rates. As manifested in Figure 5D, the C_{dl} of Mo-Cu₂S/CF (58 mF cm⁻²) is much higher than that of Cu₂S/CF (50 mF cm⁻²) and pure CF (0.04 mF cm⁻²), meaning that Mo-Cu₂S/CF possess more active surface area, generally resulting in even more active sites and normally better catalytic activity [48].

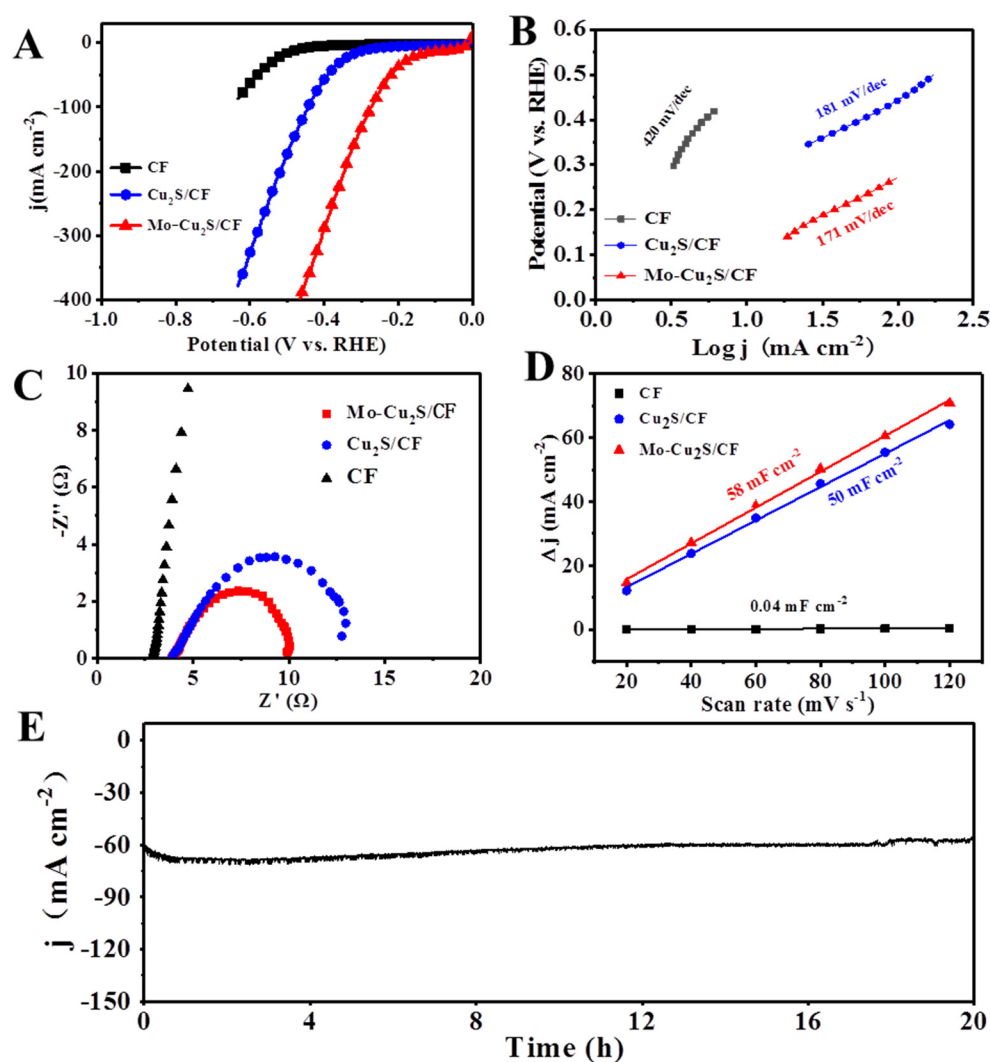


Figure 5. (A) LSV polarization curves of Mo-Cu₂S/CF, Cu₂S/CF and CF in 1.0 M KOH at scan rate of 5 mVs⁻¹; (B) Tafel curves; (C) EIS Nyquist plots; (D) C_{dl} plots for the estimation of the ECSA; (E) chronoamperometric curve (I-t) obtained for HER with Mo-Cu₂S/CF at the current density of 60 mA cm⁻² in 1 M KOH.

Meanwhile, the highly durability of Mo-Cu₂S/CF is investigated by chronopotentiometry, and Mo-Cu₂S/CF displays a negligible attenuation of overpotential after 20 h at 60 mA cm⁻², proving its excellent stability. The XRD pattern in Figure S5 signifies that the phase remains Mo-Cu₂S after 20 h HER electrocatalysis. Meanwhile, the TEM, HRTEM and elementals mapping images after 20 h HER test (Figure S6), the microstructure and composition of the catalyst were well-maintained, confirming the outstanding structural stability after long-term HER electrocatalysis.

From the above tests, it is inferred that the excellent HER activity of Mo-Cu₂S/CF has the following three aspects: (I) using foam copper (CF) as the substrate is conducive to the uniform distribution of Mo-Cu₂S on the surface, and can effectively inhibit the interlayer aggregation of the nanosheets. Besides, the “all in one” self-supporting electrode improves the catalytic stability and activity avoids the influence of the binder between the catalyst surface and the electrolyte. (II) multilayer nanosheets of Mo-Cu₂S/CF increases the contact area with electrolyte in the process of HER; this structure provides more active sites, which makes the hydrogen evolution reaction more efficient. (III) Mo doping increases the charge transfer rate, which is beneficial to the electrocatalytic process.

3. Experimental Section

3.1. Reagents and Materials

Sodium molybdate dishydrate (NaMoO₄·2H₂O) and thioacetamide (C₂H₅NS) were analytical grade and bought from Sinopharm Group Chemical Reagent Co., Ltd. (Beijing, China). KOH, C₃H₂O and CH₃CH₂OH were purchased from Tianjin Kemeiou Reagent Co., Ltd. (Tianjin, China) The copper foam (CF, with 1 mm thickness) was obtained from Suzhou Jiashide foam metal Co., Ltd. (Suzhou, China).

3.2. Synthesis of Mo-Cu₂S/CF Samples

The Mo-Cu₂S/CF samples were prepared by one-step hydrothermal method. Typically, 0.25 mmol of Na₂MoO₄·2H₂O and 1.25 mmol of C₂H₅NS were dissolved in 30 mL ultrapure water under stirring treatment. A piece of 1 cm × 5.5 cm copper foam (CF) was cleaned with acetone and 3 M hydrochloric acid for 15 min in each to remove the impurities on the surface. It was then immersed in ethanol and deionized water 5 min respectively to wash several times alternately. Subsequently, the obtained mixture was added into a 50 mL polyphenylene autoclave, which was heated at 180 °C oven for 24 h, and then cooled to indoor temperature. Finally, the resulting materials was obtained and repeatedly rinsed with water and ethanol several times, subsequently dried at 60 °C for 10 h in vacuum. In addition, so as to further investigate the impact of hydrothermal reaction time on the structure and catalytic performance, three other samples by changing the reaction time (6 h, 12 h and 36 h) were synthesized, which were denoted as Mo-Cu₂S/CF -6, Mo-Cu₂S/CF -12 and Mo-Cu₂S/CF -36.

3.3. Synthesis of Cu₂S/CF Samples

In the synthesis of Cu₂S/CF, the reaction conditions were the same as those of Mo-Cu₂S/CF, except that Na₂MoO₄·2H₂O was not added in the raw material.

3.4. Electrochemical Measurements

Relevant electrochemical measurements were conducted in a typical three-electrode electrochemical system and performed on the CHI660E B17060 electrochemical workstation (Chenhua Instrument Co., LTD. Shanghai). The as-prepared Mo-Cu₂S/CF and Cu₂S/CF served as the working electrode, as well as extremely saturated calomel reference electrode (SCE) and graphite carbon counter electrode. For the electrochemical measurements, the prepared Mo-Cu₂S/CF material exposed a 0.3 cm × 0.4 cm area as a working electrode. The HER measurements were carried out in 1 M KOH, and the potential vs. SCE was converted into reversible hydrogen electrode (RHE) according with the equation of $E_{vs\ RHE} = E_{vs\ SCE} + 0.242 + 0.059\ pH$. The linear sweep voltammetry (LSV) curve was per-

formed at the scan rate of 5 mV s^{-1} and iR-corrected. Tafel slopes were derived from the LSV curves. Electrochemical impedance spectroscopy (EIS) was measured at a voltage generated by Faraday current with a frequency range from 10^{-2} to 10^5 Hz. The stability measurement was evaluated with I-T curve under a constant voltage. Electrochemical specific surface area (ECSA) was obtained by conducting cyclic voltammetry (CV) under the different scanning speeds (20, 40, 60, 80, 100 and 120 mV s^{-1}), which is proportional to the C_{dl} and also an important factor in electrochemical measurements.

3.5. Materials Characterization

X-ray diffraction (XRD) data were performed by the Rigaku D/max-2200pc. The microstructure and morphology were monitored by field emission scanning electron microscopy (FESEM, Hitachi, S4800), the transmission electron microscopy and high-resolution TEM were tested on Tecnai G2 F20S-TWIN. X-ray photoelectron spectroscopy (XPS) was obtained on an XIS SUPRA.

4. Conclusions

In summary, a novel Mo-doped Cu_2S nanosheets ($\text{Mo-Cu}_2\text{S/CF}$) grown in situ on copper foam (CF) has been successfully synthesized by a simple one-step hydrothermal method. Experimental results provide evidence that Mo doping can regulate the catalyst morphology and modulate the electronic structure, thus enhancing the hydrogen evolution activity. The over potential is only 322 mV in the alkaline condition (1 M KOH) at current density 100 mA cm^{-2} , and the stability could be maintained for at least 20 h. Therefore, the optimized $\text{Mo-Cu}_2\text{S/CF}$ catalyst exhibiting remarkable electrocatalytic activity provides a direction for the development of transition metal sulfide self-supported electrode for HER.

Supplementary Materials: The following supporting information can be downloaded at: <https://www.mdpi.com/article/10.3390/molecules27185961/s1>, Figure S1. XRD of $\text{Mo-Cu}_2\text{S/CF}$ -6 h; $\text{Mo-Cu}_2\text{S/CF}$ -12 h; $\text{Mo-Cu}_2\text{S/CF}$ -24 h; $\text{Mo-Cu}_2\text{S/CF}$ -36 h, Figure S2. (A–C) SEM, TEM and HRTEM images, (D–F) The corresponding elementals mapping images of $\text{Cu}_2\text{S/CF}$, Figure S3. STEM-EDX spectrum of the $\text{Mo-Cu}_2\text{S/NF}$, Figure S4. Polarization curves of $\text{Mo-Cu}_2\text{S/CF}$ -6 h; $\text{Mo-Cu}_2\text{S/CF}$ -12 h; $\text{Mo-Cu}_2\text{S/CF}$ -24 h; $\text{Mo-Cu}_2\text{S/CF}$ -36 h, Figure S5. XRD of $\text{Mo-Cu}_2\text{S/CF}$ after HER test, Figure S6. (A–B) TEM and HRTEM images, (C–F) The corresponding elementals mapping images of $\text{Mo-Cu}_2\text{S/CF}$ after 20 h HER test, Table S1. The atomic percentage of the $\text{Mo-Cu}_2\text{S/NF}$, Table S2. Comparison of the electrocatalytic activity of $\text{Mo-Cu}_2\text{S}$ with previously reported Cu_2S -based electrocatalysts in 1.0 M KOH electrolyte.

Author Contributions: Conceptualization: L.F. and J.H.; methodology: Y.X. and L.F.; software: Y.X. and X.L.; validation: Y.X. and D.H.; formal analysis: Y.X.; M.N. and G.X.; investigation: Y.X.; data curation: R.X.; writing—original draft preparation: Y.X.; writing—review and editing: L.F. and J.H.; funding acquisition: J.H.; L.F.; L.C.; Y.X. and G.X. All authors have read and agreed to the published version of the manuscript.

Funding: This work was supported by the National Natural Science Foundation of China (Nos. 22179074, 52172049, 52073166), Science and Technology Resource Sharing Platform of Shaanxi Province (No.2020PT-022), Agricultural Science and Technology Innovation Drive project of Shaanxi Agricultural Department (No. NYKJ-2022-XA-08), Scientific Research Project of Education Department of Shaanxi Province (No. 22JK0297) and Open Project of Key Laboratory of Auxiliary Chemistry and Technology for Chemical Industry, Ministry of Education, Shaanxi University of Science and Technology (No. KFKT2020-06).

Conflicts of Interest: There is no conflict to declare.

References

1. Meloni, E.; Iervolino, G.; Ruocco, C.; Renda, S.; Festa, G.; Martino, M.; Palma, V. Electrified hydrogen production from methane for PEM fuel cells feeding: A review. *Energies* **2022**, *15*, 3588. [[CrossRef](#)]
2. Meloni, E.; Martino, M.; Iervolino, G.; Ruocco, C.; Renda, S.; Festa, G.; Palma, V. The route from green H_2 production through bioethanol reforming to CO_2 catalytic conversion: A Review. *Energies* **2022**, *15*, 2383. [[CrossRef](#)]

3. Mohammed-Ibrahim, J.; Sun, X. Recent progress on earth abundant electrocatalysts for hydrogen evolution reaction (HER) in alkaline medium to achieve efficient water splitting—A review. *J. Energy Chem.* **2019**, *33*, 111–160. [[CrossRef](#)]
4. Liu, Q.; Huang, J.; Cao, L.; Kajiyoshi, K.; Li, K.; Feng, Y.; Fu, C.; Kou, L.; Feng, L. V-doping triggered formation and structural evolution of dendritic Ni₃S₂@NiO core–shell nanoarrays for accelerating alkaline water splitting. *ACS Sustain. Chem. Eng.* **2020**, *8*, 6222–6233. [[CrossRef](#)]
5. Zhu, Y.; Tian, P.; Jiang, H.; Mu, J.; Meng, L.; Su, X.; Wang, Y.; Lin, Y.; Zhu, Y.; Song, L.; et al. Synergistic effect of platinum single atoms and nanoclusters boosting electrocatalytic hydrogen evolution. *CCS Chem.* **2020**, *2*, 2539–2547. [[CrossRef](#)]
6. Guan, Y.; Feng, Y.; Wan, J.; Yang, X.; Fang, L.; Gu, X.; Liu, R.; Huang, Z.; Li, J.; Luo, J.; et al. Ganoderma-like MoS₂/NiS₂ with single platinum atoms doping as an efficient and stable hydrogen evolution reaction catalyst. *Small* **2018**, *14*, 1800697. [[CrossRef](#)] [[PubMed](#)]
7. Mendoza-Garcia, A.; Su, D.; Sun, S. Sea urchin-like cobalt–iron phosphide as an active catalyst for oxygen evolution reaction. *Nanoscale* **2016**, *8*, 3244–3247. [[CrossRef](#)]
8. Ma, B.; Yang, Z.; Chen, Y.; Yuan, Z. Nickel cobalt phosphide with three-dimensional nanostructure as a highly efficient electrocatalyst for hydrogen evolution reaction in both acidic and alkaline electrolytes. *Nano Res.* **2019**, *12*, 375–380. [[CrossRef](#)]
9. Liu, M.; Li, J. Cobalt phosphide hollow polyhedron as efficient bifunctional electrocatalysts for the evolution reaction of hydrogen and oxygen. *ACS Appl. Mater. Interfaces* **2016**, *8*, 2158–2165. [[CrossRef](#)]
10. Wang, Y.; Ma, B.; Chen, Y. Iron phosphides supported on three-dimensional iron foam as an efficient electrocatalyst for water splitting reactions. *J. Mater. Sci.* **2019**, *54*, 14872–14883. [[CrossRef](#)]
11. Chen, S.; Dai, J.; Ren, F.; Xu, H.; Du, Y. 3D hollow nanoflowers assembled by ultrathin molybdenum-nickel phosphide nanosheets as robust electrocatalysts for oxygen evolution reaction. *J. Colloid Interface Sci.* **2019**, *536*, 71–79. [[CrossRef](#)] [[PubMed](#)]
12. Weng, B.; Xu, F.; Wang, C.; Meng, W.; Grice, C.; Yan, Y. Layered Na_{1-x}Ni_yFe_{1-y}O₂ double oxide oxygen evolution reaction electrocatalyst for highly efficient water-splitting. *Energy Environ. Sci.* **2017**, *10*, 121–128. [[CrossRef](#)]
13. Zhuang, L.; Ge, L.; Yang, Y.; Li, M.; Jia, Y.; Yao, X.; Zhu, Z. Ultrathin iron-cobalt oxide nanosheets with abundant oxygen vacancies for the oxygen evolution reaction. *Adv. Mater.* **2017**, *29*, 1606793. [[CrossRef](#)]
14. Zhou, W.; Lu, J.; Zhou, K.; Yang, L.; Ke, Y.; Tang, Z.; Chen, S. CoSe₂ nanoparticles embedded defective carbon nanotubes derived from MOFs as efficient electrocatalyst for hydrogen evolution reaction. *Nano Energy* **2016**, *28*, 143–150. [[CrossRef](#)]
15. Kong, D.; Wang, H.; Lu, Z.; Cui, Y. CoSe₂ nanoparticles grown on carbon fiber paper: An efficient and stable electrocatalyst for hydrogen evolution reaction. *J. Am. Chem. Soc.* **2014**, *136*, 4897–4900. [[CrossRef](#)] [[PubMed](#)]
16. Cai, P.; Huang, J.; Chen, J.; Wen, Z. Oxygen-incorporated amorphous cobalt sulfide porous nanocubes as high-activity electrocatalysts for the oxygen evolution reaction in an alkaline/neutral medium. *Angew. Chem. Int. Ed.* **2017**, *56*, 4858–4861. [[CrossRef](#)]
17. Lukowski, M.; Daniel, A.; Meng, F.; Forticaux, A.; Li, L.; Jin, S. Enhanced hydrogen evolution catalysis from chemically exfoliated metallic MoS₂ nanosheets. *J. the Am. Chem. Soc.* **2013**, *135*, 10274–10277. [[CrossRef](#)]
18. Chen, Y.; Ren, R.; Wen, Z.; Ci, S.; Chang, J.; Mao, S.; Chen, J. Superior electrocatalysis for hydrogen evolution with crumpled graphene/tungsten disulfide/tungsten trioxide ternary nanohybrids. *Nano Energy* **2018**, *47*, 66–73. [[CrossRef](#)]
19. Staszak-Jirkovský, J.; Malliakas, C.; Lopes, P.; Danilovic, N.; Kota, S.; Chang, K.; Genorio, B.; Strmcnik, D.; Stamenkovic, V.; Kanatzidis, M.; et al. Design of active and stable Co–Mo–S_x chalcogels as pH-universal catalysts for the hydrogen evolution reaction. *Nat. Mater.* **2016**, *15*, 197–203. [[CrossRef](#)]
20. Zhu, G.; Xia, G.; Yu, X. Hierarchical 3D cuprous sulfide nanoporous cluster arrays self-assembled on copper foam as a binder free cathode for hybrid magnesium-based batteries. *Small* **2021**, *17*, 2101845. [[CrossRef](#)]
21. Gong, J.; Jain, P. Room-temperature superionic-phase nanocrystals synthesized with a twinned lattice. *Nat. Commun.* **2019**, *10*, 3285. [[CrossRef](#)] [[PubMed](#)]
22. Li, Z.; Yang, B.; Lv, X.; Li, Y.; Wang, L. Synthesis of cuprous sulfide nanoparticles anchored graphene for enhanced capacitive energy storage. *Appl. Surf. Sci.* **2016**, *370*, 508–513. [[CrossRef](#)]
23. Hu, Y.; Zhang, L.; Bai, J.; Liu, F.; Wang, Z.; Wu, W.; Bradley, R.; Li, L.; Ruan, H.; Guo, S. Boosting high-rate sodium storage of CuS via a hollow spherical nanostructure and surface pseudocapacitive behavior. *ACS Appl. Energy Mater.* **2021**, *4*, 8901–8909. [[CrossRef](#)]
24. Wang, L.; Wang, Z.; Wang, L.; Yang, Z.; Zhu, Q.; Liu, Y.; Fang, W.; Gong, X.; Liu, Y.; Liu, X.; et al. CuS_x-mediated two reaction systems enable biomimetic photocatalysis in CO₂ reduction with visible light. *J. Energy Chem.* **2022**, *65*, 497–504. [[CrossRef](#)]
25. Li, J.; Yuan, L.; Li, S.; Tang, Z.; Xu, Y. One-dimensional copper-based heterostructures toward photo-driven reduction of CO₂ to sustainable fuels and feedstocks. *J. Mater. Chem. A* **2019**, *7*, 8676–8689. [[CrossRef](#)]
26. Ma, B.; Yang, Z.; Yuan, Z.; Chen, Y. Effective surface roughening of three-dimensional copper foam via sulfurization treatment as a bifunctional electrocatalyst for water splitting. *Int. J. Hydrogen Energy* **2019**, *44*, 1620–1626. [[CrossRef](#)]
27. Yang, D.; Cao, L.; Huang, J.; Liu, Q.; Li, G.; He, D.; Wang, J.; Feng, L. Vanadium-doped hierarchical Cu₂S nanowall arrays assembled by nanowires on copper foam as an efficient electrocatalyst for hydrogen evolution reaction. *Scr. Mater.* **2021**, *196*, 113756. [[CrossRef](#)]
28. Thi, L.; Din, N.; Dinh, C.; Nguyen, N.; Manh, T.; Nguyen, V.; Tac, D.; Hai, L. Three-dimensional heterostructures of Co@Cu_xS core–shell nanowire arrays as efficient bifunctional electrocatalysts for overall water splitting. *Colloids Surf. A Physicochem. Eng. Aspects* **2021**, *611*, 125779. [[CrossRef](#)]

29. Zhang, R.; Wei, Z.; Ye, G.; Chen, G.; Miao, J.; Zhou, X.; Zhu, X.; Cao, X.; Sun, X. “d-Electron Complementation” induced V-Co phosphide for efficient overall water splitting. *Adv. Energy Mater.* **2021**, *11*, 2101758. [[CrossRef](#)]
30. Adamson, W.; Jia, C.; Li, Y.; Zhao, C. Cobalt oxide micro flowers derived from hydrothermal synthesised cobalt sulphide pre-catalyst for enhanced water oxidation. *Electrochim. Acta* **2020**, *355*, 136802. [[CrossRef](#)]
31. Shen, C.; Sun, L.; Koh, Z.; Wang, Q. Cuprous sulfide counter electrodes prepared by ion exchange for high-efficiency quantum dot-sensitized solar cells. *J. Mater. Chem. A* **2014**, *2*, 2807. [[CrossRef](#)]
32. Liu, P.; Hensen, E. Highly efficient and robust Au/MgCuCr₂O₄ catalyst for gasphase oxidation of ethanol to acetaldehyde. *J. Am. Chem. Soc.* **2013**, *135*, 14032–14035. [[CrossRef](#)] [[PubMed](#)]
33. Deutsch, K.; Shanks, B. Active species of copper chromite catalyst in C–O hydrogenolysis of 5-methylfurfuryl alcohol. *J. Catal.* **2012**, *285*, 235–241. [[CrossRef](#)]
34. Severino, F.; Laine, J.; Fierro, J.; Agudo, A. Nature of Copper Active Sites in the Carbon Monoxide Oxidation on CuAl₂O₄ and CuCr₂O₄ Spinel Type Catalysts. *J. Catal.* **1988**, *177*, 82–95. [[CrossRef](#)]
35. Wang, C.; Wang, T.; Liu, J.; Zhou, Y.; Yu, D.; Kuei, J.; Han, F.; Li, Q.; Chen, J.; Huang, Y. Facile synthesis of silk-cocoon S-rich cobalt polysulfide as an efficient catalyst for hydrogen evolution reaction. *Energy Environ. Sci.* **2018**, *9*, 2467–2475. [[CrossRef](#)]
36. Guo, Y.; Zhang, X.; Zhang, X.; You, T. Defect- and S-rich ultrathin MoS₂ nanosheets embedded N-doped carbon nanofibers for efficient hydrogen evolution. *J. Mater. Chem. A* **2015**, *3*, 15927–15934. [[CrossRef](#)]
37. Deng, Z.; Li, L.; Ding, W.; Xiong, K.; Wei, Z. Synthesized ultrathin MoS₂ nanosheets perpendicular to graphene for catalysis of hydrogen evolution reaction. *Chem. Commun.* **2015**, *51*, 1893–1896. [[CrossRef](#)]
38. Hu, D.; Wang, X.; Yang, H.; Liu, D.; Wang, Y.; Guo, J.; Wu, T. Host-guest electrocatalyst with cage-confined cuprous sulfide nanoparticles in etched chalcogenide semiconductor zeolite for highly efficient oxygen reduction reaction. *Electrochim. Acta* **2018**, *282*, 877–885. [[CrossRef](#)]
39. Liu, Q.; Huang, J.; Zhao, Y.; Li, K.; Zhang, N.; Yang, D.; Feng, L.; Feng, L. Tuning coupling interface of ultrathin Ni₃S₂@NiV-LDH heterogeneous nanosheet electrocatalysts for improved overall water splitting. *Nanoscale* **2019**, *11*, 8855–8863. [[CrossRef](#)]
40. Feng, J.; Xu, H.; Dong, Y.; Ye, S.; Tong, Y.; Li, G. FeOOH/Co/FeOOH hybrid nanotube arrays as high-performance electrocatalysts for the oxygen evolution reaction. *Angew. Chem.* **2016**, *128*, 3758–3762. [[CrossRef](#)]
41. Marimuthu, T.; Yuvakkumar, R.; Ravi, G.; Zheng, Y.; Bi, Z.; Xu, X.; Xu, G.; Velauthapillai, D. One-step fabrication of copper sulfide catalysts for HER in natural seawater and their bifunctional properties in freshwater splitting. *Fuel* **2022**, *322*, 124073. [[CrossRef](#)]
42. Xie, N.; Ma, D.; Wu, Y.; Zhu, Q. Hierarchical Cu₂S hollow nanowire arrays for highly efficient hydrogen evolution reaction. *Sustain. Energy Fuels* **2021**, *5*, 2633–2639.
43. Lv, L.; Li, Z.; Wan, H.; Wang, C. Achieving low-energy consumption water-to-hydrogen conversion via urea electrolysis over a bifunctional electrode of hierarchical cuprous sulfide@nickel selenide nanoarrays. *J. Colloid Interface Sci.* **2021**, *592*, 13–21. [[CrossRef](#)] [[PubMed](#)]
44. Bhat, K.; Nagaraja, H. In Situ Synthesis of Copper Sulfide-Nickel Sulfide Arrays on Three-Dimensional Nickel Foam for Overall Water Splitting. *ChemistrySelect* **2020**, *5*, 2455–2464. [[CrossRef](#)]
45. Wang, D.; Li, J.; Xu, H.; Zhao, J. Bifunctional Cu₂S–Co(OH)₂ nanotube array/Cu foam electrocatalyst for overall water splitting. *Electrochim. Acta* **2019**, *316*, 8–18. [[CrossRef](#)]
46. Zhou, Q.; Li, T.; Wang, J.; Guo, F.; Zheng, Y. Hierarchical Cu₂S NRs@CoS core-shell structure and its derivative towards synergistic electrocatalytic water splitting. *Electrochim. Acta* **2018**, *296*, 1035–1041. [[CrossRef](#)]
47. Yang, L.; Yao, Y.; Zhu, G.; Ma, M.; Wang, W.; Wang, L.; Zhang, H.; Zhang, Y.; Jiao, Z. Co doping of worm-like Cu₂S: An efficient and durable heterogeneous electrocatalyst for alkaline water oxidation. *J. Alloys Compd.* **2018**, *762*, 637–642. [[CrossRef](#)]
48. He, D.; Cao, L.; Huang, J.; Kajiyoshi, K.; Wu, J.; Wang, C.; Liu, Q.; Yang, D.; Feng, L. In-situ optimizing the valence configuration of vanadium sites in NiV-LDH nanosheet arrays for enhanced hydrogen evolution reaction. *J. Energy Chem.* **2020**, *47*, 263–271. [[CrossRef](#)]